Multiple triaxial bands in ^{138}Nd

C. M. Petrache,[1] I. Ragnarsson,[2] Hai-Liang Ma,[3] R. Leguillon,[1,4] T. Zerrouki,[1] D. Bazzacco,[5] and S. Lunardi[5]

[1]*Centre de Sciences Nucléaires et de Sciences de la Matière, Université Paris-Sud and CNRS/IN2P3, Bât. 104-108, F-91405 Orsay, France*

[2]*Division of Mathematical Physics, LTH, Lund University, P.O. Box 118, SE-221 00 Lund, Sweden*

[3]*Department of Nuclear Physics, China Institute of Atomic Energy, Box 275(10), Beijing 102413, China*

[4]*Advanced Science Research Center, Japan Atomic Energy Agency, 2-4 Shirakata Shirane, Tokai, Ibaraki 319-1195 Japan*

[5]*Dipartimento di Fisica e Astronomia dell'Universitá and INFN Sezione di Padova, I-35131 Padova, Italy*

(Received 11 August 2014; revised manuscript received 3 December 2014; published 4 February 2015)

High-spin states in ^{138}Nd were investigated by using the ^{48}Ca + ^{94}Zr reaction and γ-ray coincidences were acquired with the GASP spectrometer. A rich level scheme was developed including 14 new bands of quadrupole transitions at very high spins. Linking transitions connecting 11 high-spin bands to low-energy states have been observed. Calculations based on the cranked Nilsson–Strutinsky formalism have been used to assign configurations to the observed bands. The main result of these calculations is that all 14 bands exhibit a stable triaxial deformation up to the highest observed spins, giving strong support to the existence of a triaxial minimum with normal deformation and positive asymmetry parameter in nuclei with a few holes in the $N = 82$ shell closure.

DOI: 10.1103/PhysRevC.91.024302 PACS number(s): 21.10.Re, 21.60.Ev, 23.20.Lv, 27.60.+j

I. INTRODUCTION

To prove that a nucleus can acquire a stable triaxial shape is not an easy task. The two degrees of freedom describing a triaxial shape are the axial quadruple deformation ε_2 and the axial asymmetry γ. In expressions of physical quantities like the transition quadrupole moment or the reduced transition probabilities, these deformation parameters appear in multiplicative factors from which one cannot extract their separate values. However, many theoretical models predict stable triaxial shape at high spin in different regions of nuclei. One example is the cranked Nilsson–Strutinsky model, which has been applied extensively to the interpretation of high-spin bands in several regions of the nuclear chart [1,2].

The triaxiality at high spins has been discussed in the Er-Lu-Hf mass region, where so-called triaxial superdeformed (TSD) bands have been established in a few nuclei and suggested in many others; see e.g., Refs. [3–7]. The prediction of triaxial bands in this mass region has been experimentally supported by the observation of wobbling bands in Lu nuclei [3]. The structure of the bands is, however, more uncertain in other nuclei, as discussed in connection with recent lifetime measurements [8,9] and in several theoretical papers, e.g., Refs. [10–14].

Another region of nuclei with stable triaxial shapes at high spins is the Nd region of nuclei with few holes in the $N = 82$ shell closure, in which many bands have been observed recently [15–19]. In contrast to the Er-Lu-Hf nuclei, which are well deformed and most of the observed structures are rotational bands built on a triaxial shape, the Nd nuclei present a variety of shapes which coexist at high spins: multiple triaxial bands were observed in ^{138,139,140}Nd [15–19], spherical isomeric states were observed in ^{139,140}Nd [20,21], a highly deformed band was observed in ^{138}Nd [22], a superdeformed (SD) band was observed in ^{140}Nd [23]. The total number of bands identified in ^{138}Nd, including the 21 bands at low and medium spins reported recently in Ref. [24], the highly deformed bands reported in Ref. [22] and the present 14 bands at high spins, amounts to 36. This is one of the highest, if not the highest, set of bands identified in a single nucleus. The level scheme of ^{138}Nd is therefore one of the better known from low to very high spins. The bands at low and medium spins have been interpreted within the framework of the tilted axis cranking (TAC) model, but random phase approximation calculations have also been performed to understand certain band structures [24]. The overall consistent description of all observed bands as configurations based on a triaxial nuclear shape strongly suggests the existence of a stable triaxial deformation at medium spin in this mass region. The high-spin bands reported in the present paper are discussed within the framework of the cranked Nilsson–Strutinsky (CNS) model and represent a nice confirmation of the theoretical calculations which predict that at high spins, the dominant configurations in ^{138}Nd are based on triaxial shapes, stabilized over extended spin ranges. Together with the high-spin triaxial bands already reported in ^{139}Nd [17] and ^{140}Nd [24], and those in ^{141}Nd that will be published soon [25], the newly observed bands in ^{138}Nd contribute to the completion of the largest set of high-spin bands observed in a restricted range of nuclei, giving thus confidence in the CNS predictions of stable triaxiality at high spins in the region of Nd nuclei with few holes in the $N = 82$ shell closure.

The present paper reports new spectroscopic information on the ^{138}Nd nucleus, for which a nearly complete level scheme at low and medium spins has been recently published [24]. Ten new bands of $E2$ transitions have been identified up to spins and excitation energy of around $45\hbar$ and 24 MeV, respectively. The four previously reported triaxial bands [15] have been extended to higher spins and linked to low-lying states, while the highly deformed band, which was observed up to spin $56\hbar$ to $58\hbar$ (depending on the spin assignment) is confirmed, but not linked to low-lying states [22]. Seven newly observed bands have been linked to low-lying states, establishing thus their excitation energies and, when possible, also their spins and parities. For three newly observed bands

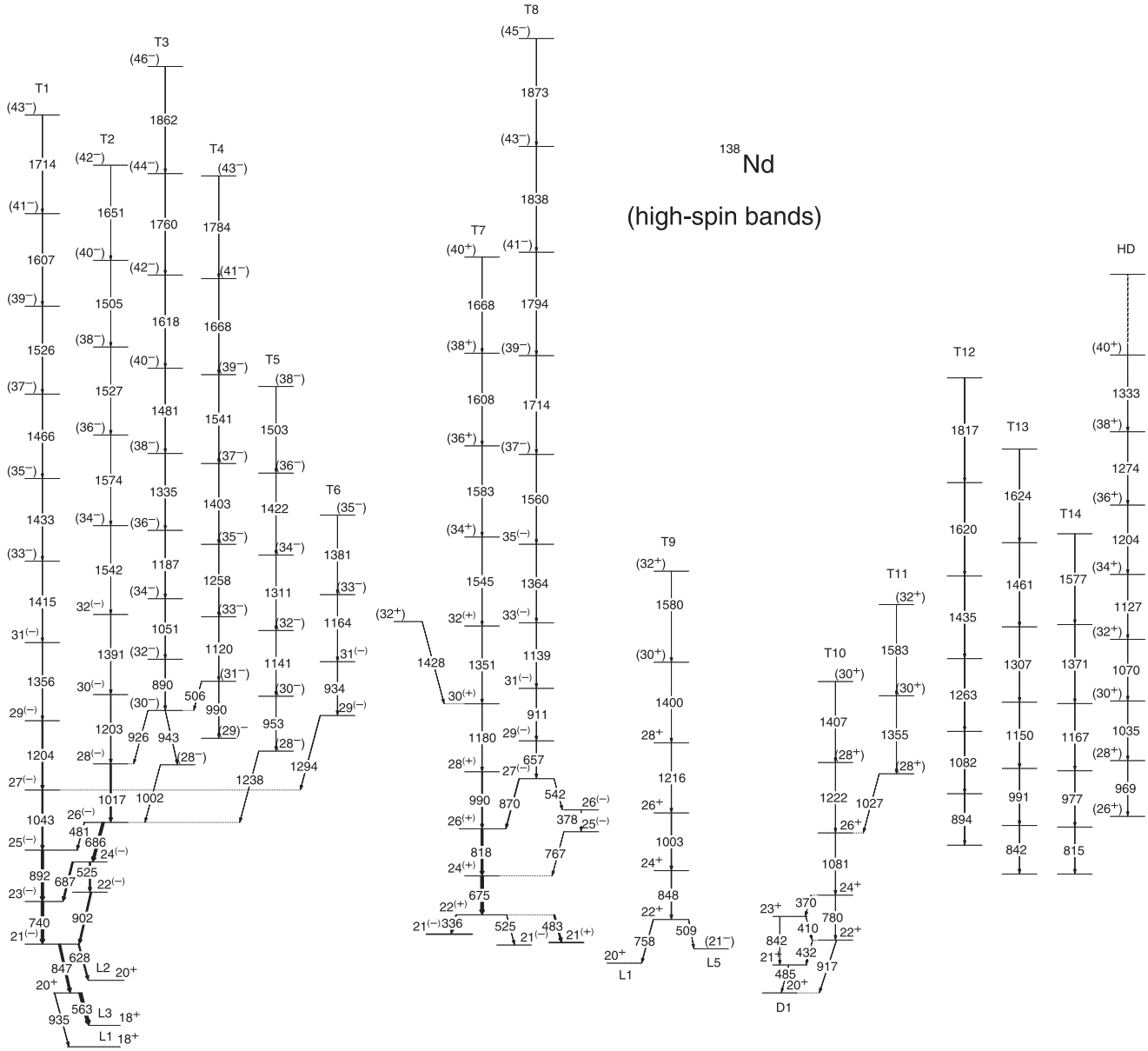

FIG. 1. Partial level scheme of ^{138}Nd showing the high-spin bands.

the excitation energy and spins are not determined because no linking transitions to low-lying states could be clearly identified.

The details of the experimental setup are briefly discussed in Sec. II. The results including the level scheme are presented in Sec. III. The configurations of the different bands are discussed in Sec. IV on the basis of theoretical calculations using the cranked-Nilsson–Strutinsky (CNS) formalism. Finally, the summary is given in Sec. V.

II. EXPERIMENTAL DETAILS

High-spin states in ^{138}Nd have been populated via the ^{48}Ca + ^{94}Zr reaction at beam energies of 188 and 195 MeV. The target consisted of a stack of two self-supporting ^{94}Zr foils of 400 μg/cm^2 thickness each. The ^{48}Ca beam of 3 to 4 pnA was provided by the XTU Tandem Accelerator of the Laboratori Nazionali di Legnaro. The Gamma Spectrometer (GASP) array with 40 Compton-suppressed Ge detectors and the 80-element BGO ball was used for a standard $\gamma-\gamma$ coincidence measurement. Events were collected when at least three suppressed Ge detectors and three BGO detectors of the inner ball fired in coincidence. A total of 1.9×10^9 triple- or higher-fold events were collected. The ^{138}Nd nucleus was one of the most intensely populated in the reaction, with about 30% of the fusion cross section.

In order to search for discrete bands we have produced a fully symmetrized cube of triple coincident γ transitions, from which we extracted doubly gated spectra for each band. The bands were assigned to ^{138}Nd on the basis of the connecting transitions with low-lying states and/or the observation in the spectra of the strong low-lying transitions

TABLE I. Energies, intensities, DCO ratios, multipolarities, and spin-parity assignments to γ-ray transitions of ^{138}Nd. The transitions are grouped in bands. The transitions connecting a band to low-lying states are given at the end of the band separated by a blank line.

γ-ray energy[a]	Intensity[b]	DCO ratios[c]		Multipolarity	$J_i^\pi \rightarrow J_f^\pi$
E_γ (keV)	I_γ (%)	Gate on $E2$	Gate on $M1$		
		Band T1			
740.3	15.5	1.10 (30)		$E2$	$23^{(-)} \rightarrow 21^{(-)}$
891.6	13.7	1.05 (35)		$E2$	$25^{(-)} \rightarrow 23^{(-)}$
1042.9	7.8	0.94 (15)		$E2$	$27^{(-)} \rightarrow 25^{(-)}$
1204.0	7	0.97 (22)		$E2$	$29^{(-)} \rightarrow 27^{(-)}$
1356.1	1.7	1.07 (30)		$E2$	$31^{(-)} \rightarrow 29^{(-)}$
1415.0	0.8	0.81 (29)		$(E2)$	$(33^-) \rightarrow 31^{(-)}$
1433.2	0.5				$(35^-) \rightarrow (33^-)$
1466.1	0.3				$(37^-) \rightarrow (35^-)$
1525.6	0.2				$(39^-) \rightarrow (37^-)$
1607.4	0.1				$(41^-) \rightarrow (39^-)$
1714.4	0.05				$(43^-) \rightarrow (41^-)$
563.2	18.8	0.92 (10)		$E2$	$20^+ \rightarrow 18^+$
628.2	7.5	0.74 (25)		$(E1)$	$21^{(-)} \rightarrow 20^+$
846.9	12.5	0.43 (20)		$(E1)$	$21^{(-)} \rightarrow 20^+$
935.0	3				$20^+ \rightarrow 18^+$
		Band T2			
524.8	7.5	1.03 (26)		$E2$	$24^{(-)} \rightarrow 22^{(-)}$
685.8	15	0.93 (20)		$E2$	$26^{(-)} \rightarrow 24^{(-)}$
1016.8	7.6	0.85 (17)		$E2$	$28^{(-)} \rightarrow 26^{(-)}$
1203.2	3.8	1.02 (15)		$E2$	$30^{(-)} \rightarrow 28^{(-)}$
1390.6	2.2	1.51 (80)		$E2$	$32^{(-)} \rightarrow 30^{(-)}$
1505.2	0.35				$(40^-) \rightarrow (38^-)$
1526.9	0.6				$(38^-) \rightarrow (36^-)$
1542.2	0.7				$(34^-) \rightarrow 32^{(-)}$
1574.4	0.5				$(36^-) \rightarrow (34^-)$
1651.2	0.2				$(42^-) \rightarrow (40^-)$
481.4	3.8	0.76 (15)		$M1/E2$	$26^{(-)} \rightarrow 25^{(-)}$
686.4	9				$24^{(-)} \rightarrow 23^{(-)}$
902.1	6.2	0.61 (15)		$M1/E2$	$22^{(-)} \rightarrow 21^{(-)}$
		Band T3			
890.1	2.5	0.85 (40)		$E2$	$(32^-) \rightarrow (30^-)$
1051.3	0.7	0.96 (35)		$E2$	$(34^-) \rightarrow (32^-)$
1187.4	0.5	1.07 (58)		$E2$	$(36^-) \rightarrow (34^-)$
1335.2	0.3				$(38^-) \rightarrow (36^-)$
1481.0	0.2				$(40^-) \rightarrow (38^-)$
1618.4	0.1				$(42^-) \rightarrow (40^-)$
1759.9	<0.1				$(44^-) \rightarrow (42^-)$
1861.7	<0.1				$(46^-) \rightarrow (44^-)$
926.1	<0.1				$(30^-) \rightarrow 28^{(-)}$
943.4	1.8	0.91 (41)		$(E2)$	$(30^-) \rightarrow (28^-)$
1001.9	0.35	0.63 (33)		$(E2)$	$(28^-) \rightarrow 26^{(-)}$
		Band T4			
989.5	0.5	1.06 (40)		$E2$	$(31^-) \rightarrow (29^-)$
1119.7	0.5	0.94 (30)		$E2$	$(33^-) \rightarrow (31^-)$
1257.8	0.2	0.76 (40)		$E2$	$(35^-) \rightarrow (33^-)$
1402.7	0.15				$(37^-) \rightarrow (35^-)$
1540.8	0.08				$(39^-) \rightarrow (37^-)$
1667.5	<0.5				$(41^-) \rightarrow (39^-)$
1783	<0.5				$(43^-) \rightarrow (41^-)$
506.4	0.5				$(31^-) \rightarrow (30^-)$

TABLE I. (*Continued.*)

γ-ray energy[a]	Intensity[b]	DCO ratios[c]		Multipolarity	$J_i^\pi \rightarrow J_f^\pi$
E_γ (keV)	I_γ (%)	Gate on $E2$	Gate on $M1$		
		Band T5			
953.1	0.9	0.93 (46)		$E2$	$(30^-) \rightarrow (28^-)$
1140.5	1.3	0.90 (30)		$E2$	$(32^-) \rightarrow (30^-)$
1311.3	0.9	0.90 (45)		$E2$	$(34^-) \rightarrow (32^-)$
1422.1	0.5	1.07 (50)		$E2$	$(36^-) \rightarrow (34^-)$
1503.2	0.2				$(38^-) \rightarrow (36^-)$
1238.1	1.6	0.97 (68)		$(E2)$	$(28^-) \rightarrow 26^{(-)}$
		Band T6			
934.2	2.7	0.92 (24)		$E2$	$(31^-) \rightarrow (29^-)$
1164.1	0.9				$(33^-) \rightarrow (31^-)$
1380.9	0.3				$(35^-) \rightarrow (33^-)$
1294.2	2.3	0.71 (22)		$(E2)$	$(29^-) \rightarrow 27^{(-)}$
		Band T7			
675.2	16.8		1.88 (19)	$E2$	$24^{(+)} \rightarrow 22^{(+)}$
817.5	11.9	1.00 (6)	2.08 (22)	$E2$	$26^{(+)} \rightarrow 24^{(+)}$
990.4	5.8	1.05 (16)	2.06 (51)	$E2$	$28^{(+)} \rightarrow 26^{(+)}$
1180.4	2.8	0.95 (12)		$E2$	$30^{(+)} \rightarrow 28^{(+)}$
1351.4	1.2	0.95 (30)		$E2$	$32^{(+)} \rightarrow 30^{(+)}$
1544.7	0.3				$(34^+) \rightarrow 32^{(+)}$
1583.2	0.2				$(36^+) \rightarrow (34^+)$
1608.0	0.1				$(38^+) \rightarrow (36^+)$
1668.1	0.05				$(40^+) \rightarrow (38^+)$
335.7	5.4		0.70 (30)	$(E1)$	$22^{(+)} \rightarrow 21^{(-)}$
483.1	8.5	0.81 (7)		$(M1/E2)$	$22^{(+)} \rightarrow 21^{(+)}$
524.9	2.0		1.27 (52)	$(E1)$	$22^{(+)} \rightarrow 21^{(-)}$
		Band T8			
657.4	2.6	0.93 (7)		$E2$	$29^{(-)} \rightarrow 27^{(-)}$
911.1	2.4	0.99 (11)		$E2$	$31^{(-)} \rightarrow 29^{(-)}$
1138.6	0.7	1.00 (25)		$E2$	$33^{(-)} \rightarrow 31^{(-)}$
1363.6	0.4	0.99 (35)		$E2$	$35^{(-)} \rightarrow 33^{(-)}$
1559.8	0.1				$(37^-) \rightarrow 35^{(-)}$
1714.1	0.05				$(39^-) \rightarrow (37^-)$
1793.5	<0.05				$(41^-) \rightarrow (39^-)$
1837.5	<0.05				$(43^-) \rightarrow (41^-)$
1873	<0.05				$(45^-) \rightarrow (43^-)$
378.4	<1	0.62 (14)		$M1/E2$	$26^{(-)} \rightarrow 25^{(-)}$
542.4	<1	0.66 (45)		$M1/E2$	$27^{(-)} \rightarrow 26^{(-)}$
767.1	<1			$(E1)$	$25^{(-)} \rightarrow 24^{(+)}$
870.3	1.0	0.53 (6)	1.36 (30)	$(E1)$	$27^{(-)} \rightarrow 26^{(+)}$
		Band T9			
848.2	3.4	0.82 (20)		$E2$	$24^+ \rightarrow 22^+$
1002.8	3.6	1.18 (24)		$E2$	$26^+ \rightarrow 24^+$
1216.1	1.7	0.79 (25)		$E2$	$28^+ \rightarrow 26^+$
1400.0	0.2				$(30^+) \rightarrow 28^+$
1580.3	<0.1				$(32^+) \rightarrow (30^+)$
508.7	1.0	0.40 (17)		$(E1)$	$22^+ \rightarrow (21^-)$
757.7	3.1	1.11 (34)		$E2$	$22^+ \rightarrow 20^+$
		Band T10			
779.5	1.4	0.94 (25)		$E2$	$24^+ \rightarrow 22^+$
1080.7	2.0	1.00 (20)		$E2$	$26^+ \rightarrow 24^+$
1222.0	0.8				$(28^+) \rightarrow 26^+$
1407.4	<0.2				$(30^+) \rightarrow (28^+)$

TABLE I. (*Continued.*)

γ-ray energy[a]	Intensity[b]	DCO ratios[c]		Multipolarity	$J_i^\pi \rightarrow J_f^\pi$
E_γ (keV)	I_γ (%)	Gate on $E2$	Gate on $M1$		
369.8	1.6	0.25 (25)		$M1/E2$	$24^+ \rightarrow 23^+$
410.4	0.9	0.33 (6)		$M1/E2$	$23^+ \rightarrow 22^+$
431.5	0.5	0.27 (15)		$M1/E2$	$22^+ \rightarrow 21^+$
485.4	0.3				$21^+ \rightarrow 20^+$
841.8	1.4				$23^+ \rightarrow 21^+$
917.1	2.3	1.08 (20)		$E2$	$22^+ \rightarrow 20^+$
		Band T11			
1354.9	0.8				$(30^+) \rightarrow (28^+)$
1583.3	0.3				$(32^+) \rightarrow (30^+)$
1026.7	1.3	1.15 (40)		$(E2)$	$(28^+) \rightarrow 26^+$
		Band T12			
894.4	0.8				
1082.3	1.0				
1263.2	1.3				
1434.7	1.0				
1620.4	0.6				
1817	<0.1				
		Band T13			
842.1	2				
991.2	2				
1149.7	2.2				
1307.0	1.3				
1461.0	1.4				
1623.8	0.3				
		Band T14			
814.9	1				
976.9	1				
1167.0	0.5				
1371.3	0.4				
1577.1	0.3				
		Band HD[d]			
968.9	0.18				
1035.2	0.20				
1070.2	0.23				
1127.3	0.40				
1204.1	0.69				
1273.5	0.90				
1333.2	0.80				
1400.8	0.78				
1467.0	0.78				
1540.0	0.50				
1619.3	0.45				
1707.5	0.30				
1797.1	0.23				
1898.8	0.08				
1994	0.06				

[a]The error on the transition energies is 0.2 keV for transitions below 1000 keV and intensities larger than 5% of the ^{138}Nd reaction channel, 0.5 keV for transitions above 1000 keV and intensities lower than 5%, and 1 keV for transitions above 1200 keV and/or weaker than 1%.
[b]Relative intensities corrected for efficiency. The transition intensities were obtained from a combination of total projection and gated spectra.
[c]The DCO ratios have been deduced from an asymmetric $\gamma - \gamma$ coincidence matrix. The tentative spin parity of the states is given in parentheses.
[d]From Ref. [22].

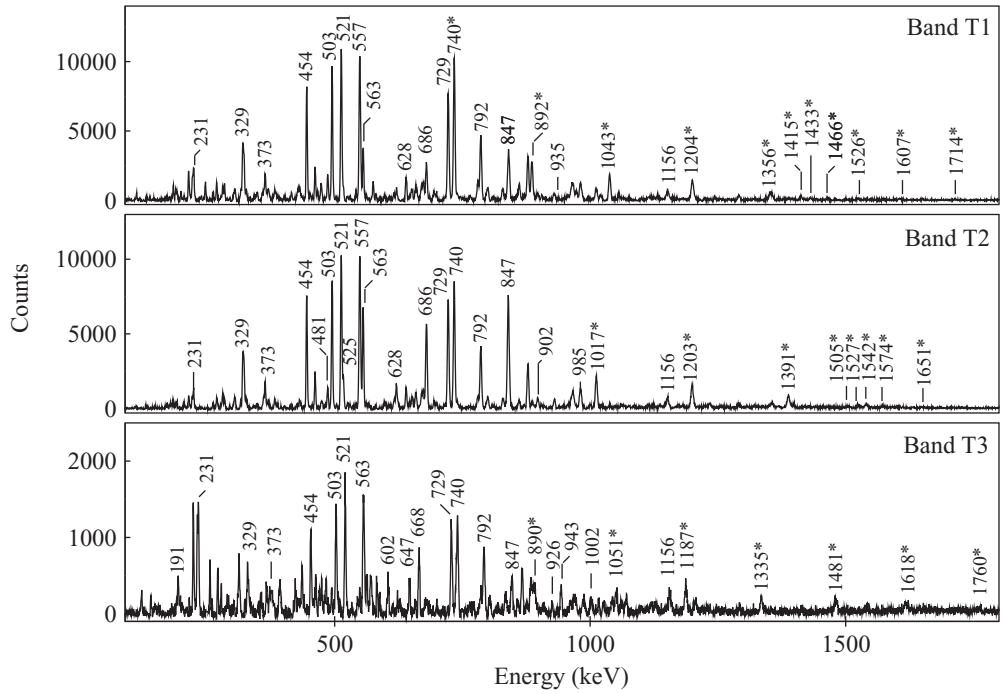

FIG. 2. Doubly gated sum spectra for the bands T1–T3 in ^{138}Nd. The gates were set on selected transitions of each band. The transitions marked with asterisks represent the members of the band.

of ^{138}Nd. The transition multipolarities were extracted from the directional correlation of oriented states (DCO) ratios by using the procedure described in Ref. [26]. The DCO ratios in the present experiment are expected to be 0.5 for pure $\Delta I = 1$ transitions and 1 for $\Delta I = 2$ transitions when gating on $\Delta I = 2$ transitions.

III. RESULTS AND LEVEL SCHEME

The high-spin part of the ^{138}Nd level scheme is shown in Fig. 1. The highly deformed band, which was observed up to spin $56\hbar$ to $58\hbar$ [22], is only shown up to spin $40\hbar$. The energies, relative intensities, DCO ratios, and spin-parity assignments of the observed transitions are reported in Table I. Doubly gated spectra for the different bands are given in Figs. 2–5.

The bands T1, T2, T7, and T8 have been observed for the first time in an 8π experiment [15]. The bands T1 and T2 were also discussed in a recent paper [19], in which results from the GASP experiment were reported. We confirm all previously observed transitions for these four bands. However, several changes were necessary at the bottom of the bands, which lead to energy and spin-parity assignments which are different than those reported in Ref. [15]. The decay of bands T1 and T2,

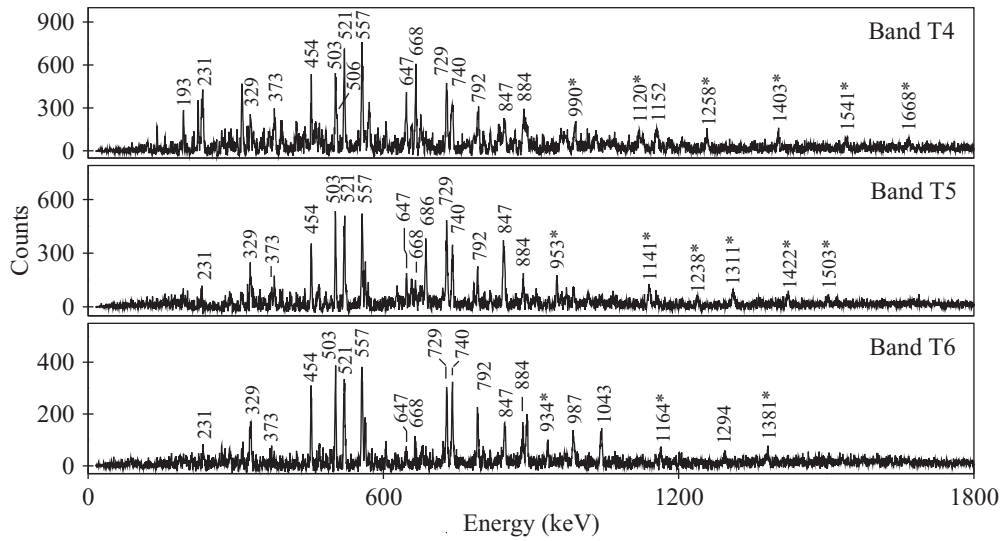

FIG. 3. The same as Fig. 2, but for bands T4–T6 in ^{138}Nd.

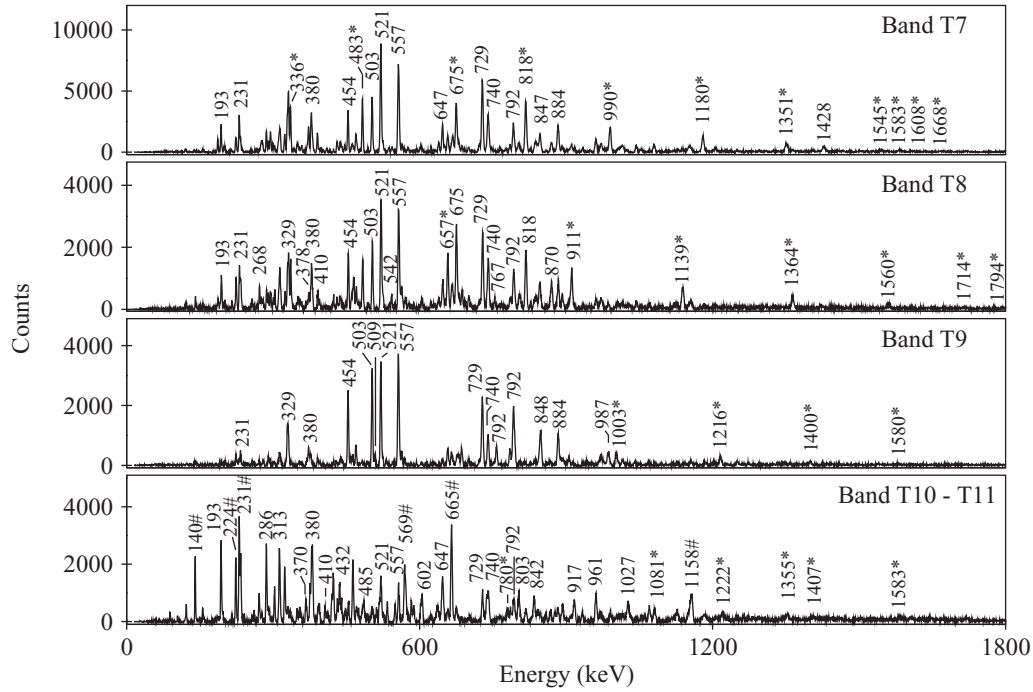

FIG. 4. The same as Fig. 2, but for bands T7–T11 in ^{138}Nd. The peaks marked with "#" are contaminants from other nuclei.

as well as their high-spin transitions, have been discussed in Ref. [19] and will not be presented here. In the present paper we report the results on the bands T3–T14. Several bands have been extended to much higher spin and excitation energy than previously reported [15]. The spins of the bands have been established based on the DCO ratios. When the DCO ratios could not be extracted or the errors of the DCO ratios were too large to establish a definite character of the transitions, the spin of the initial state of a given transition was put in parentheses. The electric or magnetic character of a transition having a DCO ratio compatible with pure $\Delta I = 1$ transitions could not be deduced from present data. The parity of a given state deexcited by a $\Delta I = 1$ transition is then put in parentheses. The parities indicated in parentheses in Fig. 1 and in Table I are the preferred parities resulting from the configuration assignment based on CNS calculations (see Sec. IV).

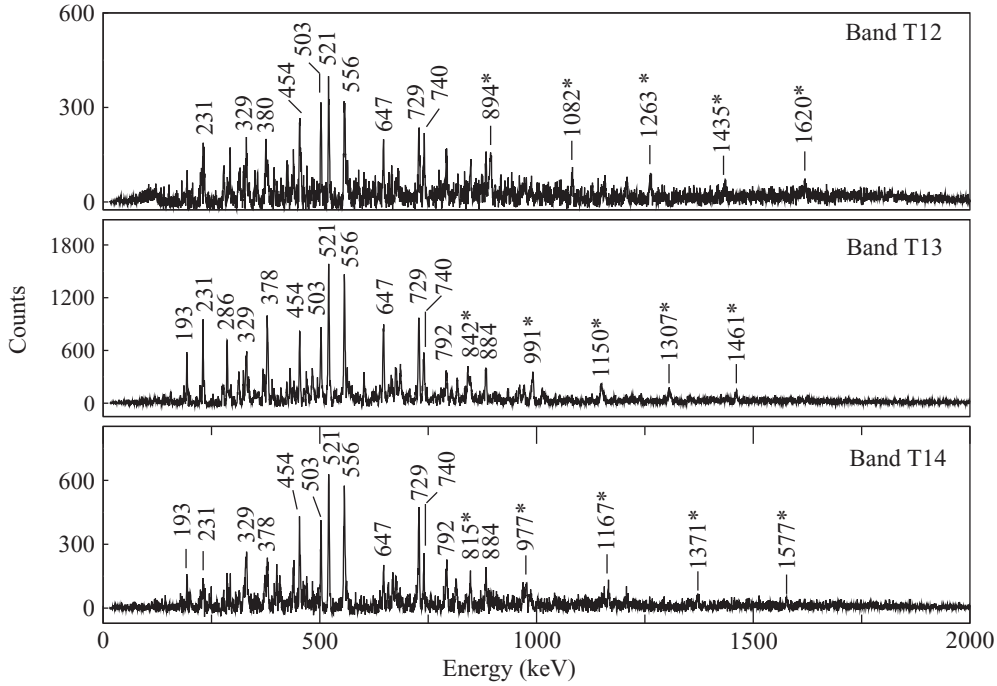

FIG. 5. The same as Fig. 2, but for bands T12–T14 in ^{138}Nd.

IV. DISCUSSION

The high-spin bands in ^{138}Nd will be analyzed by using the configuration-dependent cranked Nilsson–Strutinsky (CNS) method [1,2,27]. In this formalism, configurations of ^{138}Nd are naturally specified relative to a ^{132}Sn core as

$$\pi\left[(g_{7/2}d_{5/2})^{p_1}_{\alpha_1}(h_{11/2})^{p_2}_{\alpha_2}\right] \times \nu\left[(d_{3/2}s_{1/2})^{-n_1}_{\alpha_3}(h_{11/2})^{-n_2}_{\alpha_4}(h_{9/2}f_{7/2})^{n_3}_{\alpha_5}(i_{13/2})^{n_4}_{\alpha_6}\right]. \quad (1)$$

In this expression, the number of particles or holes in orbitals dominated by a specific j shell(s) is indicated by a superscript, while the signature is specified by α_i. A configuration is then fully specified as

$$[(p_1)_{\alpha_1}(p_2)_{\alpha_2}, (n_1)_{\alpha_3}(n_2)_{\alpha_4}\{(n_3)_{\alpha_5}(n_4)_{\alpha_6}\}].$$

The low-energy configurations have (i) $\alpha = 0$ for an even number of particles and (ii) the favored signature for an odd number of the high-j $h_{11/2}$ protons and $i_{13/2}$ neutrons, $\alpha = -1/2$ and $\alpha = +1/2$, respectively. These labels are thus suppressed while α_i is written as $+$ and $-$ for signatures $\alpha = +1/2$ and $\alpha = -1/2$, respectively.

Such labels were previously introduced for ^{140}Nd [18]. Alternatively, it is often instructive to use the less-complete labels,

$$[p_2,n_2(n_3n_4)],$$

which is the standard choice in most previous studies [1,28].

A. General features of observed bands

The observed bands are shown relative to a rotating liquid drop reference in Fig. 6, where the energy curves have a parabola-like shape.

It is instructive to draw these bands also as I vs E_γ, like in Fig. 7. In such a diagram the bands show up as approximately straight lines, with a relatively small slope, which translates into a $\mathcal{J}^{(2)}$ moment of inertia much smaller than the rigid-body value. If the lines in the I vs E_γ plot are extrapolated to smaller values of $E_\gamma = 0$, they reach the $E_\gamma = 0$ line (the no-rotation line because $\omega = E_\gamma/2$) at a large value of the spin I. This corresponds to a large alignment, i.e., several high-j particles which become strongly aligned at very low frequencies. As discussed previously [15–18], the high-j particles in these Nd isotopes are the $h_{11/2}$ protons and the neutrons which are excited to the orbitals built on the $h_{9/2}f_{7/2}$ and $i_{13/2}$ subshells above the $N = 82$ gap. The large number of aligned particles are naturally combined with a triaxial shape [15–18], i.e., the bands are formed at triaxial shape with $\gamma = 30°-35°$ and $\varepsilon_2 = 0.2-0.3$.

For most of the bands, the energy curves in Fig. 6 vary smoothly, corresponding to an approximately straight line in Fig. 7. Such bands are interpreted as built on a single configuration. Other bands show some discontinuity, corresponding to a jump in I in Fig. 7, indicating an alignment, a configuration change and/or a shape change. Such discontinuities lead to important constraints when trying to interpret the bands. For example, the discontinuity in bands T1 and T2 were interpreted as caused by shape changes in Ref. [19]. Furthermore, according to the analyses below, it appears that the discontinuities in bands T7 and T8 are also caused by shape changes, although much less pronounced and more gradual than for bands T1 and T2. Then, except for a small up bend at the highest spin values in band T5, the other

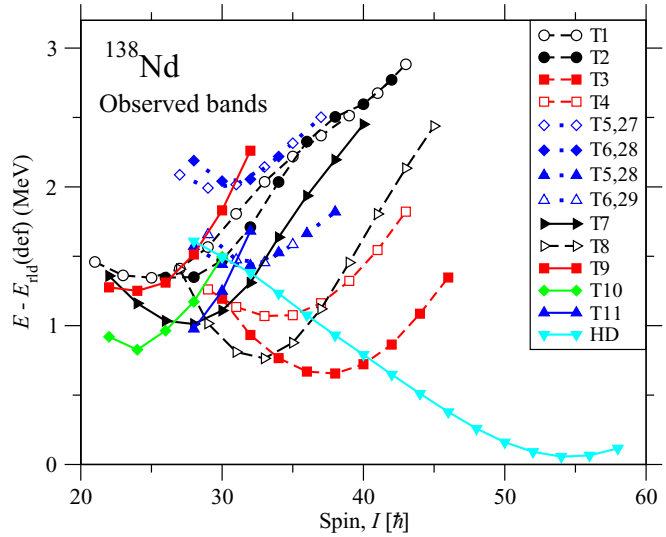

FIG. 6. (Color online) The energy of the observed and linked to low-lying states high-spin bands in ^{138}Nd are drawn relative to a rotating liquid drop energy. In addition, the HD band [22] is drawn at an arbitrary excitation energy and with tentative spin values. Full lines are used for positive-parity states and dashed lines for negative-parity states; closed symbols are used for the signature $\alpha = 0$ and open symbols for $\alpha = 1$. Dotted lines are used for the bands T5 and T6 which are drawn with two alternative spin values specified in the legend.

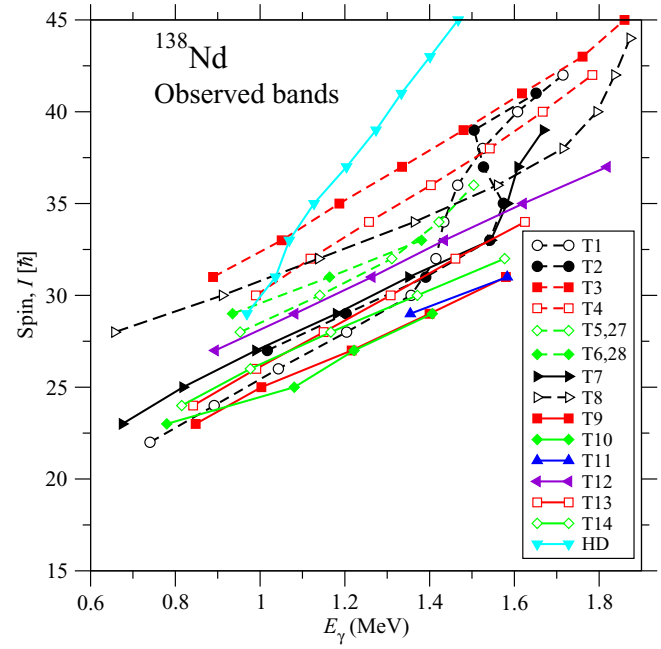

FIG. 7. (Color online) The spin values I of the observed high-spin bands in ^{138}Nd vs transition energy E_γ. For bands T5 and T6, where two spin values are suggested, only the lower values are used, with the "band-head spin" specified in the legend. The unlinked bands T12–T14 (and HD) are included with tentative spin values.

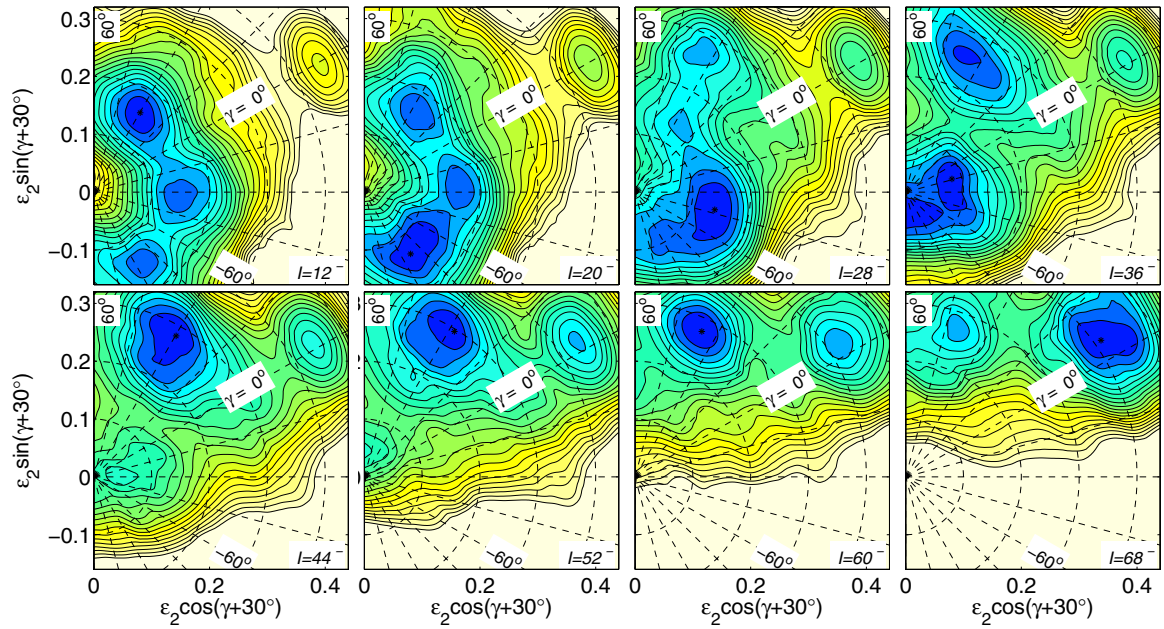

FIG. 8. (Color online) Calculated potential-energy surfaces with $(\pi,\alpha) = (-,0)$ for ^{138}Nd. The contour-line separation is 0.25 MeV.

T bands evolve smoothly in the observed spin range. This is also the case for the bands T12, T13, and T14 which are shown only in Fig. 7. Because these bands are not linked to low-lying states, we do not try to interpret them, but it is clear that they should be assigned to the same type of configurations as the other T bands.

B. Typical yrast configurations with increasing spin

Selected total-energy surfaces with positive parity and even spin (signature $\alpha = 0$) are shown in Fig. 8. At low spin there is one triaxial minimum in each of the three sectors, corresponding to approximately the same shape but with rotation around each of the three principal axes. These minima are formed in the favored neutron configuration corresponding to the triaxial $N = 78$ gap in Fig. 9, i.e., with two $\mathcal{N} = 4$ holes and two $h_{11/2}$ holes below the spherical $N = 82$ gap.

The total energy minima in ^{138}Nd are similar to those in the isotone ^{142}Gd [29]. However, while the corresponding minima appear to lead to three distinct bands in ^{142}Gd, they result in tilted-axis rotational bands in ^{138}Nd, according to Ref. [24].

In the energy surface for $I = 28^-$ shown in Fig. 8, a local minimum is formed at $\varepsilon_2 \approx 0.27$, $\gamma \approx 35^\circ$. The configurations in this minimum are formed with neutrons excited from the $\mathcal{N} = 4$ and $h_{11/2}$ orbitals just below the triaxial $N = 78$ gap in Fig. 9. They are excited to the strongly aligned orbitals in the subshells above the $N = 82$ spherical gap: two orbitals of $h_{9/2}f_{7/2}$ character and one of $i_{13/2}$ character, as is more clearly seen in Fig. 11 of Ref. [18]. In addition, the protons in $h_{11/2}$ orbitals are also easy to align; see Fig. 11 of Ref. [18]. The configurations with four high-j particles and negative parity are shown relative to a rotating liquid drop reference in Fig. 10. In this figure one notes that a large number of such configurations are calculated in the yrast region. Therefore, with an uncertainty in the calculated energies of 0.5 to 1.0 MeV, many configurations have to be considered when trying to find those which can be assigned to the observed bands.

Coming back to the energy surfaces shown in Fig. 8, in the spin range $I \approx 40-50$, the typical configurations in the triaxial minimum at positive γ have a neutron excited also to the second $\nu i_{13/2}$ orbital. It is configurations of this type which were assigned to the highly deformed band in Ref. [22]. At even higher spin values in this minimum, a proton is excited to the lowest $\pi i_{13/2}$ orbital. At $I = 60$, the minimum at $\varepsilon_2 \approx 0.40$, $\gamma \approx 0^\circ$ starts to become competitive. It appears that the superdeformed band in ^{140}Nd is built from configurations in this minimum [23].

C. Shell effects inducing triaxial shape

The triaxial gap at $N = 78$ in Fig. 9 appears to be responsible for the formation of triaxial configurations in ^{138}Nd and neighboring nuclei. Starting from the prolate shape, this gap is formed because of the coupling between the $\mathcal{N} = 4$, $n_z = 0$ orbitals by the operator generating triaxiality, $r^2(Y_{22} + Y_{2-2})$ [30]. This mechanism was first discussed in connection with the inner fission barrier in Ref. [31]. More recently [4], it was pointed out that it is because of this mechanism that triaxial highly deformed configurations are formed along a shell energy valley in the (Z,N) plane, including the nuclei ^{158}Er, ^{163}Lu, and ^{168}Hf [14]. In these nuclei, the interaction is within the same $\mathcal{N} = 4$, $n_z = 0$ orbitals as in Fig. 9, i.e., the triaxial bands in $^{138-140}$Nd constitute a continuation of the shell energy valley [4] toward smaller particle numbers, $Z \sim 60$, $N \sim 78$, and smaller deformation, $\varepsilon_2 \approx 0.20 - 0.30$. It is also interesting to note that, starting from the oblate side in Fig. 9, the $h_{11/2}$ orbitals are found around the Fermi surface. These orbitals develops towards the $\mathcal{N} = 5$, $n_z = 0$ asymptotic states with increasing oblate deformation, i.e., the orbitals with small values of n_z, which couples strongly by

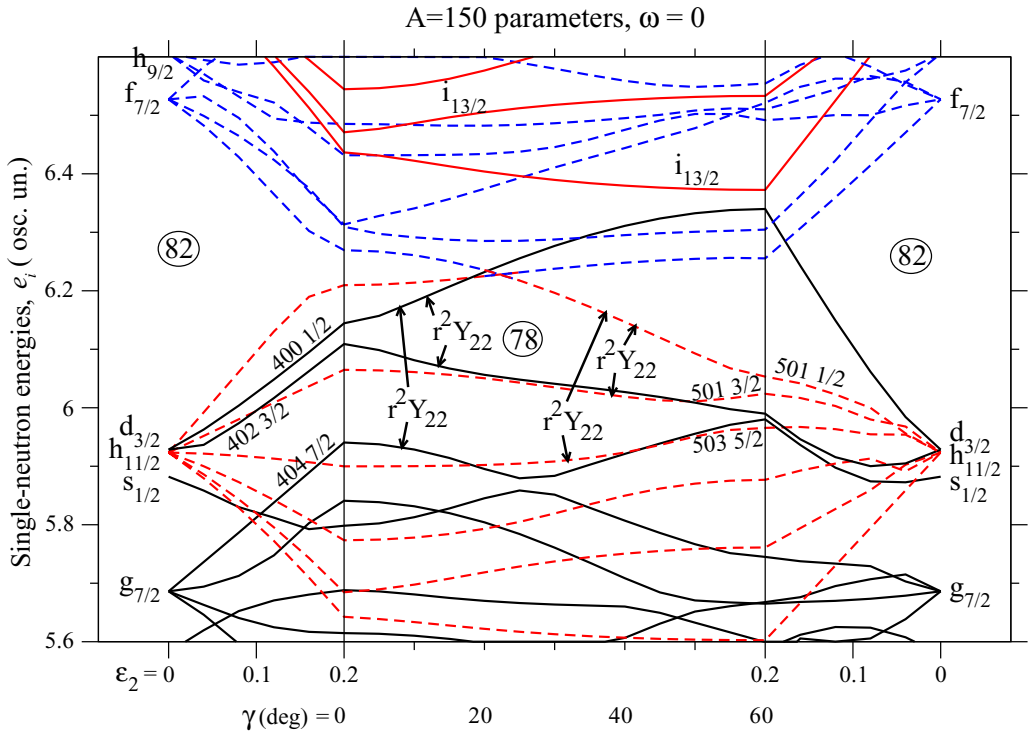

FIG. 9. (Color online) Single-neutron orbitals at no rotation and with $A = 150$ Nilsson parameters drawn first as a function of ε_2 at prolate shape ($\gamma = 0^\circ$), then as function of γ at a fixed quadrupole deformation $\varepsilon_2 = 0.2$, and finally at oblate shape ($\gamma = 60^\circ$) as function of decreasing ε_2 back to spherical shape. Full (dashed) lines are used for positive-parity (negative-parity) orbitals. Colors are used to make an approximate distinction between orbitals of high-j and low-j character, respectively. Note the interaction between the $n_z = 0$, N=4 orbitals on the prolate side ($\gamma \approx 0^\circ$ to 20°) and the interaction between the $n_z = 0$, $h_{11/2}$ orbitals on the oblate side ($\gamma \approx 40^\circ$ to 60°) leading to the triaxial N=78 gap.

the $r^2(Y_{22} + Y_{2-2})$ operator [31]. Thus, the two highest $h_{11/2}$ orbitals will split apart with increasing triaxiality, giving a complementary understanding of the triaxial $N = 78$ gap.

D. Calculations with pairing included

In addition to the unpaired CNS calculations, we also carried out calculations in the CNSB formalism with pairing included [29,32]. By varying the total energy with respect to the pairing gaps and Fermi levels, a self-consistent solution of the Hamiltonian with the monopole pairing is achieved by the CNSB model. Both the collective and noncollective states can be studied in the same framework on a deformation mesh. Because the minima on the potential-energy surfaces are at most times stable with or without pairing correlations, a direct comparison of the CNSB and CNS results would give a general impression on the pairing correction energies. In the CNSB formalism it is straightforward to fix the parity and signature for protons and neutrons separately but not to impose any further constraint on the configurations, hence altogether 16 configurations can be constructed. The same $A = 150$ Nilsson parameters are adopted in the CNSB calculations. The highly triaxial deformed shapes are developed for all 16 configurations for $I \gtrsim 25$. We then carried out CNS calculations with the same constraints and searched for the bands around the local minimum at $(\varepsilon_2, \gamma) \approx (0.27, 35^\circ)$, the same as that in the CNSB calculations. The CNS and CNSB results are compared in Fig. 11. Although the pairing correlations are strongly dependent on the configurations at low spins, for yrast bands only the first band crossing is important, as demonstrated in Ref. [32]. In Fig. 11, it is evident that in the spin range shown, $I = 25 - 60$, the general features of the different configurations are essentially the same and the pairing correction energies vary smoothly as a function of spin. Thus, the main effect of pairing is an energy gain which decreases with increasing spin. A simple fitting to the pairing correction energies can cover quite a large spin range, as shown in Figs. 11(c) and 11(f), where the magenta line gives the fitting results $\tilde{E}_{\rm pair} = -3.05\exp(-I/23.5)$ MeV.

E. Configuration assignments for the T bands

As noted previously [18], the number of high-j particles or, more exactly, the maximum spin contribution from the high-j particles, is strongly correlated to the minimum in the $E - E_{rld}$ plots. Thus, minima of the configurations with three high-j particles are located at $I \approx 20-25$, while they are located at $I \approx 25-32$ for the configurations with four high-j particles (see Fig. 10), and at $I \approx 32-40$ for the configurations with five high-j particles. These general rules about the position of the minima gives a good first idea about the configurations that can be assigned to the experimental bands.

The energies of the observed bands T1, T2, T3, and T4 and the calculated configurations assigned to them are compared in Fig. 12. In this and the following figures, where observed and calculated bands are compared, pairing is included

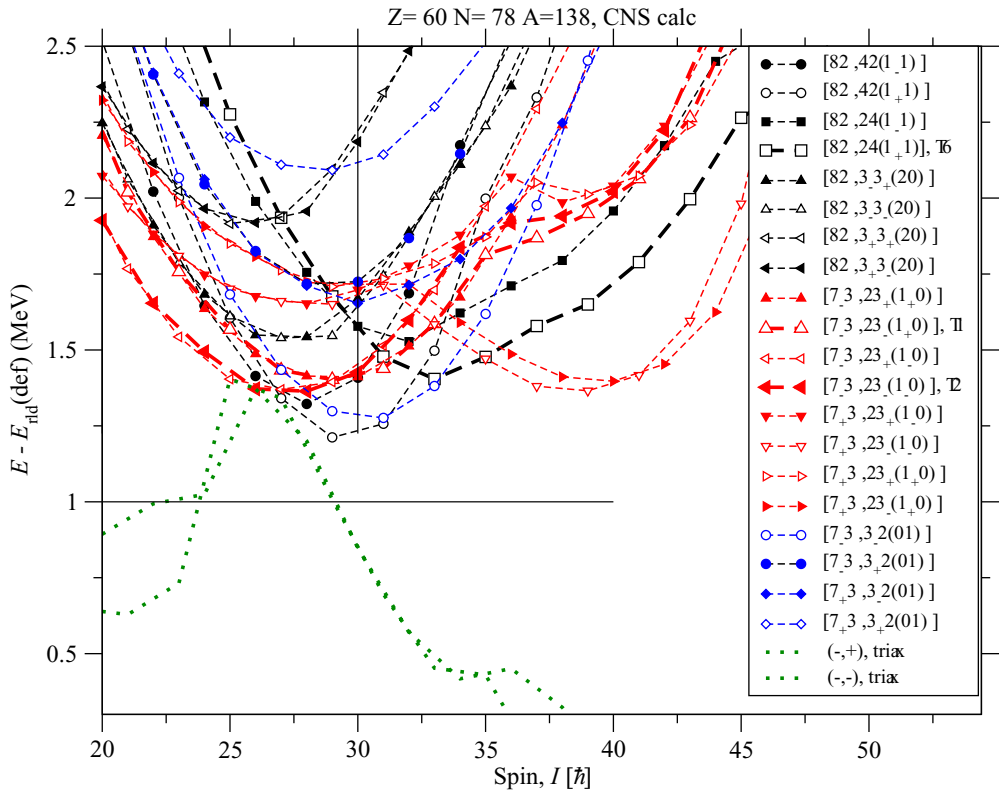

FIG. 10. (Color online) Energies relative to a standard rotating liquid drop reference calculated for configurations with negative parity and four high-j particles, i.e., two or three protons in $h_{11/2}$ and two or one neutrons excited above $N = 82$. The labeling of the configurations is explained in the text. With an odd number of $h_{11/2}$ neutron holes, two signature degenerate bands are formed which are shown by the same color and symbols. Configurations assigned to the observed bands are shown by thicker lines and larger symbols. The negative-parity yrast lines of both signatures at triaxial shape for $\gamma > 0^\circ$ are shown by dotted lines. Note that the observed bands are generally predicted to be rather high above yrast in most of their observed spin range.

in an average sense, because the energy $\tilde{E}_{\rm pair} = -3.05\exp(-I/23.5)$ MeV (see Fig. 11) is added to the calculated CNS energies. The T1 and T2 bands were discussed in Ref. [19], where the general agreement between experiment and calculations over an extended spin range gives strong evidence for the present assignments, which are specified in Table II. Note that with the average pairing energy added to the calculated CNS energies in Fig. 12, the difference between experiment and calculations is rather constant as a function of spin. The fact that the difference is not zero, but rather around -1 MeV, is not unexpected, being comparable, for example, with typical values for the smooth terminating bands in the $A = 110$ region [2].

The relative spins of bands T3 and T4 are fixed, but the spin values could vary by $1\hbar$. Considering that the bands should be close to yrast, the higher spin values appear more plausible. Furthermore, with the lower spin values, it is difficult to find any reasonable assignment with configurations which are not too different from that of band T2 to which band T3 decays. With the higher spin values and with the configuration assignments specified in Table II, a nice agreement between calculations and experiment is obtained, as seen in Fig. 12. The fact that the difference between calculations and experiment is approximately constant and almost overlapping for the two bands shows that we have found a consistent interpretation.

The shape trajectories of a few selected configurations are shown in Fig. 13. All the configurations follow the typical trend of fixed configurations approaching the noncollective axis at $\gamma = 60^\circ$ with increasing spin. However, in the spin range $I = 30-40$ where these bands are observed, their deformation is rather constant at $\varepsilon_2 \approx 0.2$, $\gamma \approx 30^\circ$. This is of course not the case for the bands T1 and T2 (only band T1 is shown in Fig. 13) which jumps to a negative value of γ at $I \approx 35$ as discussed in Ref. [19]. The shape trajectory for the configuration assigned to band T3 is very regular, resulting in a smooth energy curve in Fig. 12, while the trajectory for the configuration assigned to band T4 is somewhat less regular, resulting in some small discontinuities around $I = 45$ in Fig. 12.

The bands T5 and T6 are linked to the bands T1 and T2, respectively. The two bands T5 and T6 decay in a very similar way to bands T2 and T1, respectively, by transitions which could be either $\Delta I = 1$ or $\Delta I = 2$. Because they will become close to signature degenerate if both transitions are either $\Delta I = 1$ or $\Delta I = 2$, we will assume that this is the case, even though it cannot be excluded that one is $\Delta I = 1$ and the other $\Delta I = 2$. The two bands will come at a rather high excitation energy for $\Delta I = 1$, which suggests that the higher spin values should be chosen, i.e., $I = 28^-$ and $I = 29^-$ for the lowest observed states. The parity is chosen as $\pi = -$ because $M2$ transitions are strongly hindered and thus very unlikely.

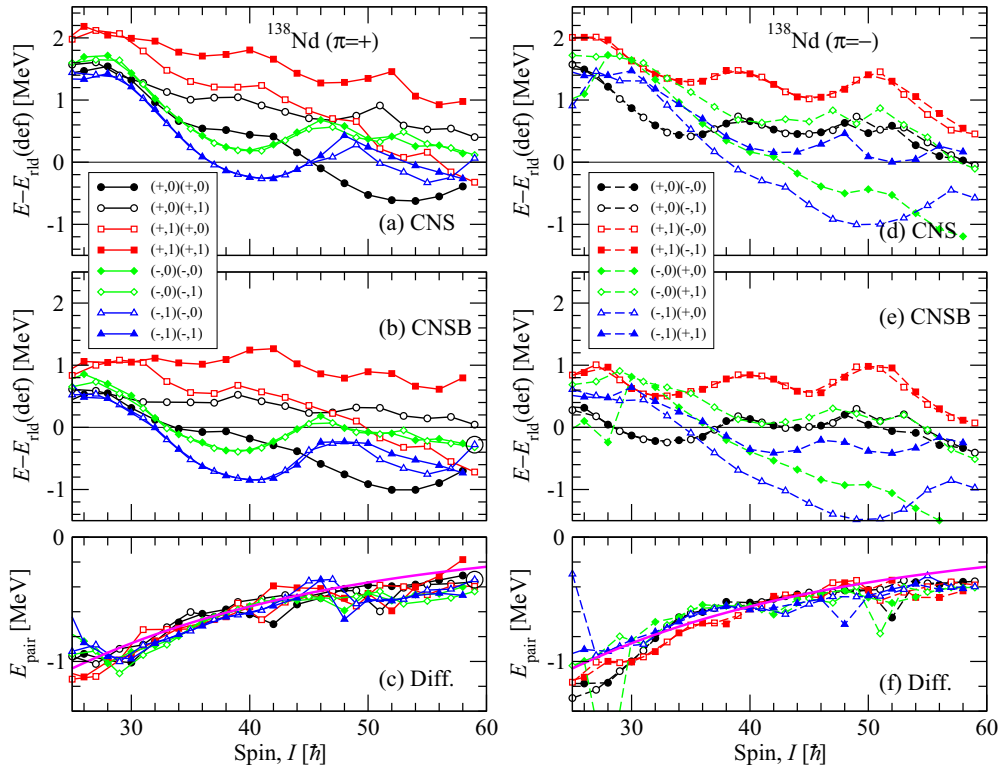

FIG. 11. (Color online) Calculated configurations at triaxial shape $(\varepsilon_2,\gamma) \approx (0.27,35^\circ)$ for 16 different parity-signature combinations are drawn relative to the rotating liquid drop energy. The left and right panels are for positive and negative parity, respectively. The energy differences between the CNS and CNSB results, interpreted as pairing corrections, are shown in panels (c) and (f). The magenta lines denote the average pairing corrections.

Comparing with the calculated states, the only reasonable assignment is then $[82,24(1_{\mp}1)]$. As seen in Fig. 14, this gives a difference between experiment and calculations in the range $[-0.8, -0.6]$ and close to constant as a function of spin, which is exactly what would be expected. It is also satisfying that the T5 and T6 bands are signature partners in the same sense as the bands T1 and T2, i.e., involving the signature $\alpha = \pm 1/2$ of the $\nu(h_{9/2}f_{7/2})$ neutron orbital. On the other hand, the configurations of the bands T1, T2 and T5, T6 differ on both the neutron and proton side, which should not favor the linking of these bands. Furthermore, we will find below that $[82,24(1_{+}1)]$ is clearly the preferred configuration for the more intense band T8, which would then exclude that this configuration should be assigned to band T6.

It appears impossible to find any other reasonable configuration which can be assigned to bands T5 and T6 if the linking transitions to bands T1 and T2 are assumed to be stretched $E2$s. Therefore, we have also investigated which could be the possible assignments for $\Delta I = 1$ linking transitions, in which case we are also free to choose the parity. Looking for configurations with their minima at the correct spin value, which are not too high in energy and which are not too different from the configurations assigned to T1 and T2, the best choice is clearly $[7_{-}3,3_{-}3_{\pm}(20)]$ with positive parity. As seen in Fig. 14, the energy difference in the lower panel is rather constant as a function of spin, but it comes close to -2 MeV, which is another indication that the bands are placed at a higher energy than would be expected, i.e., with these spin values, the experimental bands are too high above yrast.

The spin values for bands T7 and T8 are fixed, while the parities are uncertain. Therefore, the shape of the $E-E_{rld}$ curve is fixed. As one can see in Fig. 15, the energy increase at high spin is relatively slow for both bands. This indicates some kind of band crossing at $I \approx 36$, as is more clearly seen in the I vs E_γ diagram of Fig. 7. While there are many configurations with the energy minimum at essentially the same spin value as the observed bands, most of them do not go through any band-crossing. Note also that the configurations of the two bands should be relatively similar, because they are linked with a $\Delta I = 1$ transition. The two pairs of configurations which appear to best reproduce the experimental shapes on average are listed in Table II. They are drawn in the middle panel of Fig. 15, with the difference between experiment and calculations in the lower panel. All these configurations experience a discontinuity caused by a crossing between the fourth and fifth low-j, $\mathcal{N} = 4$, $\alpha = 1/2$ orbitals, which is illustrated in Fig. 10 of Ref. [18]. However, as seen from the configurations drawn by (red) squares in Fig. 15, this crossing alone corresponds only to a small alignment. Thus, the trend of increasing energy difference in the lower panel of Fig. 15 shows that this crossing alone cannot explain the relatively low energies at high spin in the observed bands T7 and T8. For the configurations drawn by (black) circles on the other hand, the high-spin states are built at a similar energy as for the observed bands. It appears that this lowering of the

TABLE II. Configuration assignment to the high-spin bands of ^{138}Nd. The parity of the configurations are also indicated by "+" or "−" superscripts, while the even or odd spins of the configurations are indicated by "e" or "o" subscripts.

Band	Intensity (%)	Band head I^π	$I_{\min}$	Decay	Configuration	Alternative band head I^π and configuration
T1	15.5	$21^{(-)}$	25	L1, L2, L3	$[7_-3,23_-(1_+0)]^-_o$	
T2	7.6	$26^{(-)}$	28	T1	$[7_-3,23_-(1_-0)]^-_e$	
T3	2.5	(30^-)	38	T2	$[7_-3,3_-3_+(1_+1)]^-_e$	
T4	0.5	(29^-)	33	T3	$[7_-3,24(20)]^-_o$	
T5	1.3	(28^-)	32	T2	$[82,24(1_-1)]^-_e$	(27^+), $[7_-3,3_-3_+(20)]^+_o$
T6	2.7	(29^-)	33	T1	$[82,24(1_+1)]^+_o$	(28^+), $[7_-3,3_-3_-(20)]^+_e$
T7	16.8	$22^{(+)}$	28	$\pi = -$	$[82,24(20)]^+_e$	$22^{(-)}$, $[82,3_-3_+(20)]^-_e$
T8	2.6	$27^{(-)}$	33	T7	$[82,24(1_+1)]^-_o$	$27^{(+)}$, $[82,3_-3_+(1_+1)]^+_o$
T9	3.6	22^+	26	L1, L5	$[82,42(20)]^+_e$	See Fig. 16
T10	2	22^+	26	D1	$[7_-3,3_-2(1_-0)]^+_e$	See Fig. 16
T11	0.8	(28^+)	<28	T10	$[7_-3,3_+2(1_+0)]^+_e$	See Fig. 16

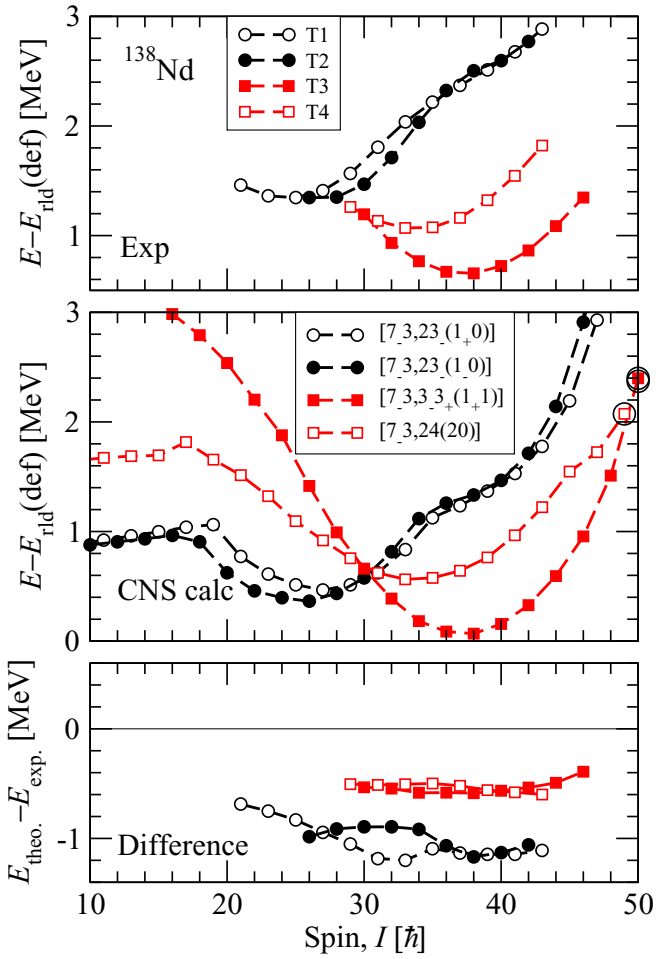

FIG. 12. (Color online) The observed bands T1, T2, T3, and T4 in ^{138}Nd are shown relative to a rotating liquid drop reference in the upper panel, with the calculated configurations assigned to these bands shown relative to the same reference in the middle panel. Aligned states are encircled. In the calculated bands, an average pairing energy (see Fig. 11) is added. The lower panel shows the difference between calculations and experiment. Full (open) lines are used for positive (negative) parity and closed (open) symbols for signature $\alpha = 0$ ($\alpha = 1$).

energy at high spin is caused by rather important shape changes towards smaller ε_2 values, as illustrated for the $[82,24(1_+1)]$ configuration assigned to band T8 in Fig. 13. With these preferred assignments for bands T7 and T8, the differences in the lower panel of Fig. 15 are on the average rather constant, while the local variations result because the discontinuities in the energy curves come at somewhat different spin values for the observed bands and for the configurations assigned to them.

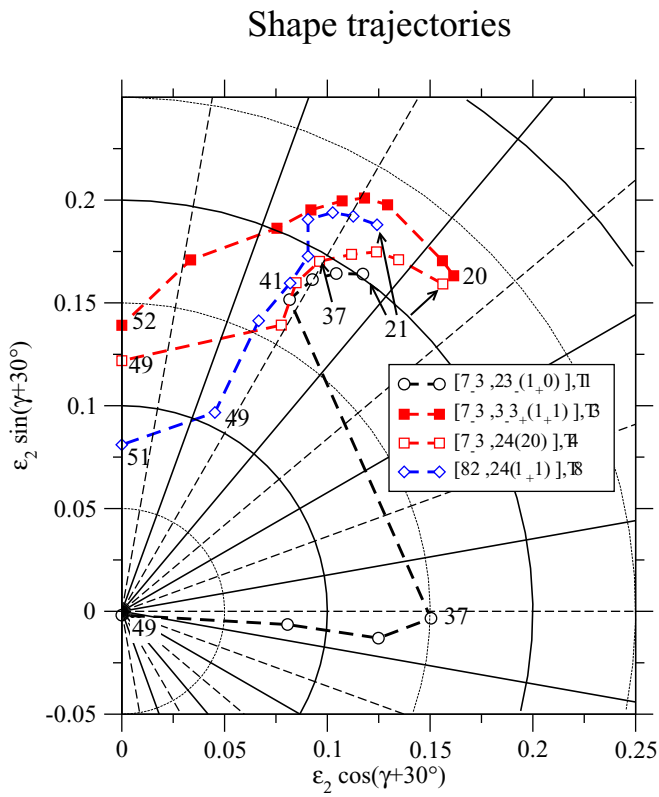

FIG. 13. (Color online) Calculated shape trajectories for the configurations assigned to the bands T1, T3, T4, and T8.

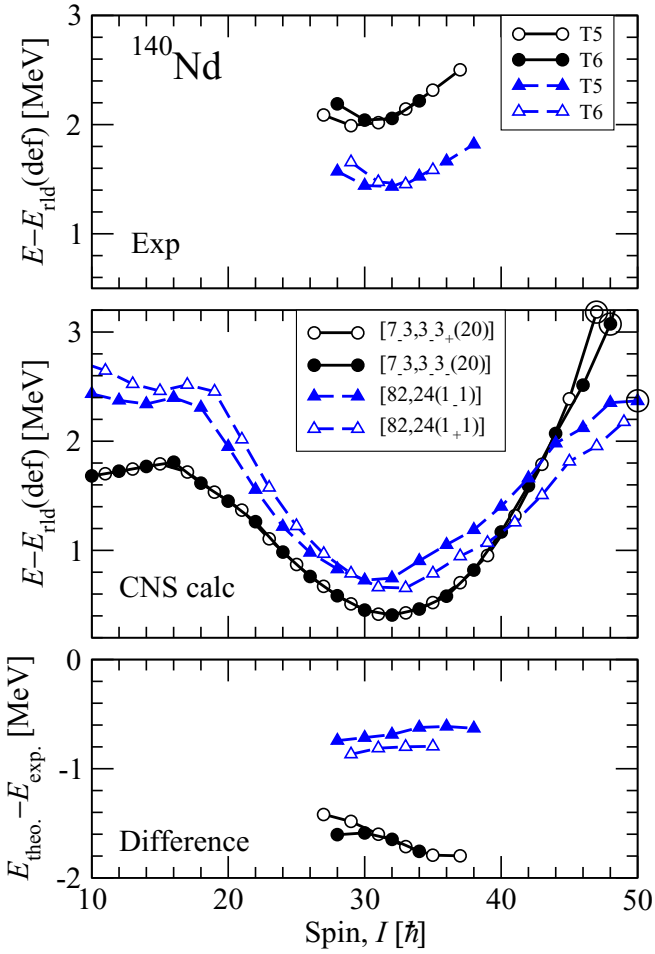

FIG. 14. (Color online) Same as Fig. 12 for the bands T5 and T6 with two different spin values and corresponding assignments for the two bands.

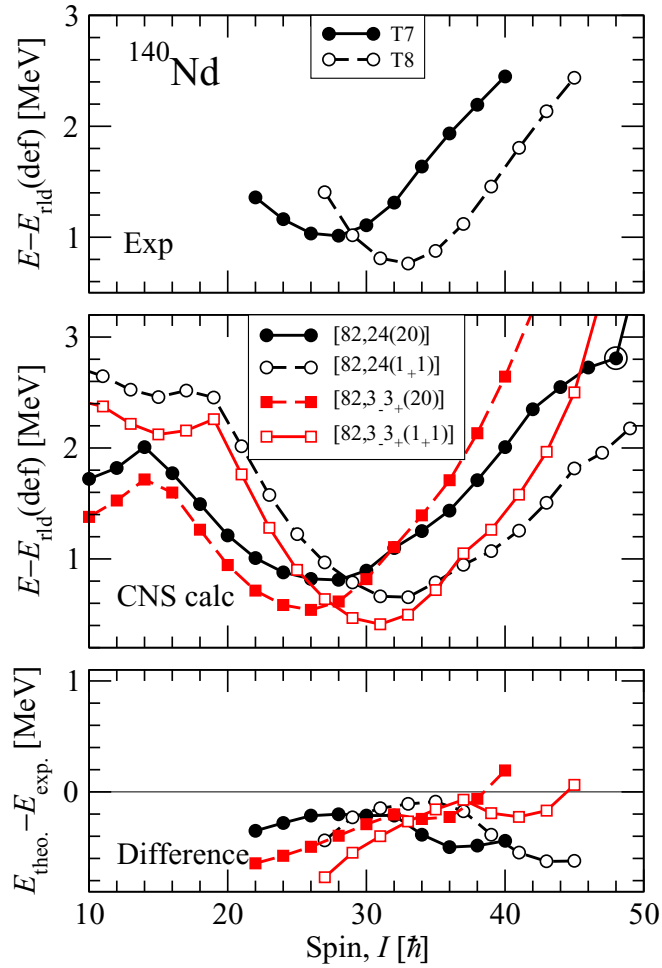

FIG. 15. (Color online) Same as Fig. 12 but for the bands T7 and T8. The two observed bands are drawn with their preferred parities, but possible assignments are also presented for the two bands having opposite parity.

The bands T9 and T10 have fixed even spins and positive parity. Both of them have their energy minima in the $E-E_{rld}$ curves close to $I = 24$. There are several calculated configurations with similar minima which are drawn in the middle panel of Fig. 16. Considering the linking to the lower spin states, we concluded that the bands T9 and T10 are most naturally assigned to the configurations listed in Table II. With these assignments, the difference between observed and calculated energies is drawn in the lower panel of Fig. 16. Band T11 is seen in a very short spin interval with no minimum in the $E-E_{rld}$ curve. This means that any assignment becomes very tentative. However, assuming that it is linked to band T10 by a stretched $E2$ transition, it is reproduced pretty well by the same type of configurations as those of the bands T9, T10. It is compared with such a configuration in Fig. 16. With this interpretation, however, it appears strange that it is not observed in a more extended spin range.

F. Features at highest spin values

It is interesting to investigate the maximum spin and possible terminations of the configurations assigned to the bands T1–T11. Some of the calculated configurations are followed to termination in the middle panels of Figs. 12, 14, 15, and 16. However, most of these terminations are far above yrast and will probably be very difficult to observe. Band T3 might be an exception because, with the present interpretation, it is observed only two transitions short of termination. The configurations, whose shape trajectories are drawn in Fig. 13, reach the noncollective $\gamma = 60^\circ, -120^\circ$ axis at $I_{\max} \approx 50$. Their $I_{\max}$ value is calculated with the $\mathcal{N} = 4$ protons confined to the $(d_{5/2}g_{7/2})$ orbitals. The $\mathcal{N} = 4$ neutron holes are distributed not only over the $(d_{3/2}s_{1/2})$ orbitals, but also over the $(d_{5/2}g_{7/2})$ orbitals. However, for the configurations which terminate at oblate shape with $\varepsilon_2 \gtrsim 0.10$, the [440] $\frac{1}{2}$ Nilsson orbital comes at a high energy, as seen in a standard Nilsson diagram. As a consequence, two of the $\mathcal{N} = 4$ holes are placed in this orbital, not contributing to the spin.

With the present assignments, most differences in the lower panels of Figs. 12, 14, 15, and 16 come in the range $[-1,0]$ MeV and they are rather constant as a function of spin, as expected in the present CNS calculations with a schematic pairing energy included. An unexpected feature, however,

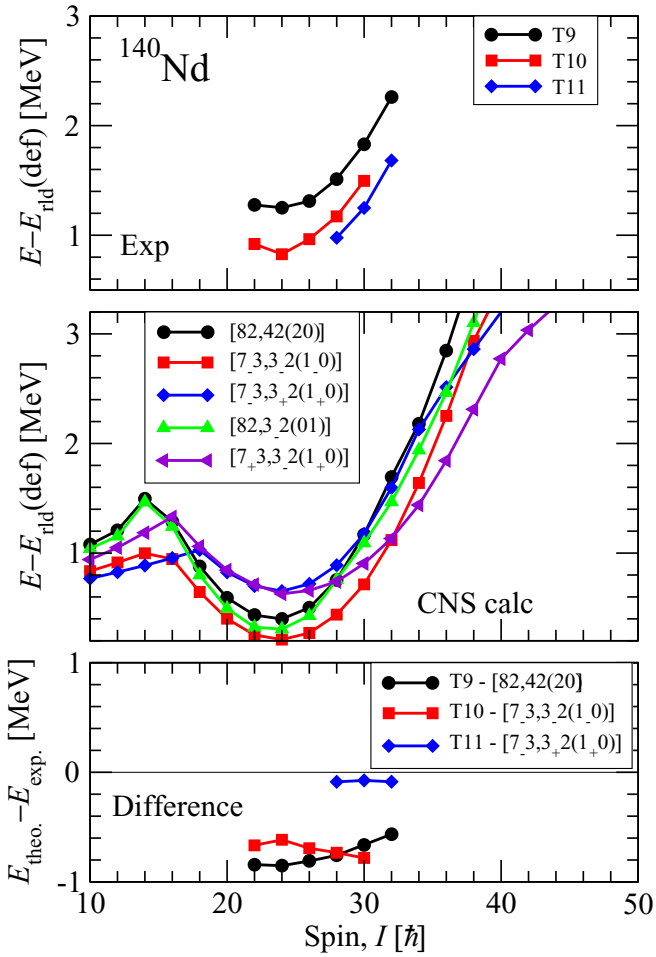

FIG. 16. (Color online) Same as Fig. 12 but for the observed bands T9, T10, and T11. In addition to our preferred assignments, two more possible configurations are shown in the middle panel.

is that some of the observed bands appear to be around 3 MeV above yrast for $I \approx 40$. Considering that the parities and spin values of many of the observed bands are uncertain, it would be important to get more firm link of the present bands, maybe observe them to higher spin values and try to observe other bands at somewhat higher spin values where the yrast states appear to be more favored in energy. In this context, it would of course also be important if the HD band could be linked, so that its excitation energy and spin values could be determined. In view of the fact that some of the bands have a relatively high intensity, it seems that it would be possible to get such a better understanding of the triaxial bands in ^{138}Nd (and neighboring nuclei) from an experiment at the present state-of-the-art facilities.

V. SUMMARY

Fourteen high-spin bands of quadrupole transitions have been observed in ^{138}Nd by using the ^{48}Ca + ^{94}Zr reaction and the GASP spectrometer to measure γ-ray coincidences. The linking transitions to low-lying states were identified for 11 bands, allowing the assignment of excitation energy, and in some cases also the spins and parity. The bands have been interpreted by using the cranked Nilsson–Strutinsky formalism. The comparison between calculations and experiment give strong evidence that these bands are built on triaxial configurations with $\varepsilon_2 = 0.20-0.30$, $\gamma = 30^\circ$ to 40°, involving 3 to 5 high-j particles distributed over the $\pi h_{11/2}$, $\nu(h_{9/2}f_{7/2})$, and $\nu i_{13/2}$ subshells. On the other hand, except for two bands which are observed only up to $I \sim 30$, it has not been possible to experimentally determine both the spin values and the parity of these bands. Furthermore, some of the configurations which have been assigned to the bands reach spin values which are surprisingly high above yrast. These facts put some doubts on the present assignments, suggesting that more experimental information is needed to get a definite understanding of the high-spin structure of ^{138}Nd. Indeed, a high statistics experiment using a thin target and a state-of-the-art facility should allow us to establish the spins and parities for the majority of the observed bands, to extend some bands to higher spins, to observe more bands at higher spin values, and possibly to link the highly deformed band to low-lying states. In addition to this, it would be very useful to measure the lifetimes of the states in as many as possible high-spin bands.

[1] A. V. Afanasjev, D. B. Fossan, G. J. Lane, and I. Ragnarsson, Phys. Rep. **322**, 1 (1999).
[2] B. G. Carlsson and I. Ragnarsson, Phys. Rev. C **74**, 011302 (2006).
[3] S. W. Ødegård, G. B. Hagemann, D. R. Jensen, M. Bergström, B. Herskind, G. Sletten, S. Törmänen, J. N. Wilson, P. O. Tjøm, I. Hamamoto, K. Spohr, H. Hübel, A. Görgen, G. Schönwasser, A. Bracco, S. Leoni, A. Maj, C. M. Petrache, P. Bednarczyk, and D. Curien, Phys. Rev. Lett. **86**, 5866 (2001).
[4] E. S. Paul, P. J. Twin, A. O. Evans, A. Pipidis, M. A. Riley, J. Simpson, D. E. Appelbe, D. B. Campbell, P. T. W. Choy, R. M. Clark, M. Cromaz, P. Fallon, A. Görgen, D. T. Joss, I. Y. Lee, A. O. Macchiavelli, P. J. Nolan, D. Ward, and I. Ragnarsson, Phys. Rev. Lett. **98**, 012501 (2007).
[5] K. Lagergren *et al.*, Phys. Rev. Lett. **87**, 022502 (2001).
[6] R. B. Yadav *et al.*, Phys. Rev. C **78**, 044316 (2008).
[7] J. Ollier *et al.*, Phys. Rev. C **80**, 064322 (2009).
[8] X. Wang *et al.*, Phys. Lett. B **702**, 127 (2011).
[9] J. P. Revill *et al.*, Phys. Rev. C **88**, 031304(R) (2013).
[10] Y. C. Zhang, W. C. Ma, A. V. Afanasjev, G. B. Hagemann, J. Begnaud, M. P. Carpenter, P. Chowdhury, D. M. Cullen, M. K. Djongolov, D. J. Hartley, R. V. F. Janssens, T. L. Khoo, F. G. Kondev, T. Lauritsen, E. F. Moore, E. Ngijori-Yogo, S. W. Ødegard, L. L. Riedinger, S. V. Rigby, D. G. Roux, D. T. Scholes, R. B. Yadav, J. Y. Zhang, and S. Zhu, Phys. Rev. C **76**, 064321 (2007).
[11] H.-L. Ma, B.-G. Dong, and Y.-L. Yan, Chin. Phys. Lett. **25**, 3928 (2008).

[12] Y. Shi, J. Dobaczewski, S. Frauendorf, W. Nazarewicz, J. C. Pei, F. R. Xu, and N. Nikolov, Phys. Rev. Lett. **108**, 092501 (2012).
[13] A. V. Afanasjev, Y. Shi, and W. Nazarewicz, Phys. Rev. C **86**, 031304(R) (2012).
[14] A. Kardan, I. Ragnarsson, H. Miri-Hakimabad, and L. Rafat-Motevali, Phys. Rev. C **86**, 014309 (2012).
[15] C. M. Petrache, G. Lo Bianco, D. Ward, A. Galindo-Uribarri, P. Spolaore, D. Bazzacco, T. Kröll, S. Lunardi, R. Menegazzo, C. Rossi Alvarez, A. O. Macchiavelli, M. Cromaz, P. Fallon, G. J. Lane, W. Gast, R. M. Lieder, G. Falconi, A. V. Afanasjev, and I. Ragnarsson, Phys. Rev. C **61**, 011305(R) (1999).
[16] C. M. Petrache, M. Fantuzi, G. Lo Bianco, D. Mengoni, A. Neusser-Neffgen, H. Hübel, A. Al-Khatib, P. Bringel, A. Bürger, N. Nenoff, G. Schönwasser, A. K. Singh, I. Ragnarsson, G. B. Hagemann, B. Herskind, D. R. Jensen, G. Sletten, P. Fallon, A. Görgen, P. Bednarczyk, D. Curien, G. Gangopadhyay, A. Korichi, A. Lopez-Martens, B. V. T. Rao, T. S. Reddy, and Nirmal Singh, Phys. Rev. C **72**, 064318 (2005).
[17] S. Bhowal *et al.*, Phys. Rev. C **84**, 024313 (2011).
[18] R. Leguillon, C. M. Petrache, T. Zerrouki, T. Konstantinopoulos, K. Hauschild, A. Korichi, A. Lopez-Martens, S. Frauendorf, I. Ragnarsson, P. T. Greenlees, U. Jakobsson, P. Jones, R. Julin, S. Juutinen, S. Ketelhut, M. Leino, P. Nieminen, M. Nyman, P. Peura, P. Rahkila, P. Ruotsalainen, M. Sandzelius, J. Saren, C. Scholey, J. Sorri, J. Uusitalo, H. Hübel, A. Neußer-Neffgen, A. Al-Khatib, A. Bürger, N. Nenoff, A. K. Singh, D. Curien, G. B. Hagemann, B. Herskind, G. Sletten, P. Fallon, A. Görgen, P. Bednarczyk, and D. M. Cullen, Phys. Rev. C **88**, 014323 (2013).
[19] C. M. Petrache, I. Ragnarsson, Hai-Liang Ma, R. Leguillon, T. Konstantinopoulos, T. Zerrouki, D. Bazzacco, and S. Lunardi, Phys. Rev. C **88**, 051303(R) (2013).
[20] C. M. Petrache, R. A. Bark, S. T. H. Murray, M. Fantuzi, E. A. Lawrie, S. Lang, J. J. Lawrie, S. M. Maliage, D. Mengoni, S. M. Mullins, S. S. Ntshangase, D. Petrache, T. M. Ramashidzha, and I. Ragnarsson, Phys. Rev. C **74**, 034304 (2006).
[21] A. Vancraeyenest, C. M. Petrache, D. Guinet, P. T. Greenlees, U. Jakobsson, R. Julin, S. Juutinen, S. Ketelhut, M. Leino, M. Nyman, P. Peura, P. Rahkila, P. Ruotsalainen, J. Saren, C. Scholey, J. Sorri, J. Uusitalo, P. Jones, C. Ducoin, P. Lautesse, C. Mancuso, N. Redon, O. Stezowski, P. Desesquelles, R. Leguillon, A. Korichi, T. Zerrouki, D. Curien, and A. Takashima, Phys. Rev. C **87**, 064303 (2013).
[22] S. Lunardi, D. Bazzacco, C. A. Ur, M. Axiotis, G. de Angelis, E. Farnea, T. Kröll, S. M. Lenzi, G. Lo Bianco, N. Marginean, T. Martinez, R. Menegazzo, D. R. Napoli, P. Pavan, C. M. Petrache, B. Quintana, C. Rossi Alvarez, A. Saltarelli, R. Venturelli, and I. Ragnarsson, Phys. Rev. C **69**, 054302 (2004).
[23] A. Neußer, H. Hübel, A. Al-Khatib, P. Bringel, A. Bürger, N. Nenoff, G. Schönwasser, A. K. Singh, C. M. Petrache, G. Lo Bianco, I. Ragnarsson, G. B. Hagemann, B. Herskind, D. R. Jensen, G. Sletten, P. Fallon, A. Görgen, P. Bednarczyk, D. Curien, G. Gangopadhyay, A. Korichi, A. Lopez-Martens, B. V. T. Rao, T. S. Reddy, and N. Singh, Phys. Rev. C **70**, 064315 (2004).
[24] C. M. Petrache, S. Frauendorf, M. Matsuzaki, R. Leguillon, T. Zerrouki, S. Lunardi, D. Bazzacco, C. A. Ur, E. Farnea, C. Rossi Alvarez, R. Venturelli, and G. de Angelis, Phys. Rev. C **86**, 044321 (2012).
[25] T. Zerrouki *et al.* (unpublished).
[26] C. M. Petrache, D. Bazzacco, S. Lunardi, C. Rossi Alvarez, G. de Angelis, M. De Poli, D. Bucurescu, C. A. Ur, P. B. Semmes, and R. Wyss, Nucl. Phys. A **597**, 106 (1996).
[27] T. Bengtsson and I. Ragnarsson, Nucl. Phys. A **436**, 14 (1985).
[28] A. V. Afanasjev and I. Ragnarsson, Nucl. Phys. A **591**, 387 (1995).
[29] B. G. Carlsson, I. Ragnarsson, R. Bengtsson, E. O. Lieder, R. M. Lieder, and A. A. Pasternak, Phys. Rev. C **78**, 034316 (2008).
[30] S. E. Larsson, Phys. Scr. **8**, 17 (1973).
[31] S. E. Larsson, P. Möller, and S. G. Nilsson, Phys. Scr. **10A**, 53 (1974).
[32] Hai-Liang Ma, B. G. Carlsson, I. Ragnarsson, and H. Ryde, Phys. Rev. C **90**, 014316 (2014).